Progress Report Item No. 0001A

Award No. N00014-12-M-0147

Reporting Period: April 15, 2012 to September 27, 2012

Attached is the *Gear Fatigue Diagnostics and Prognostics* project progress report for the performance period noted above.

……..
Nenad G. Nenadic, PhD

Research Associate Professor, Golisano Institute for Sustainability
Principal Investigator
Rochester Institute of Technology
111 Lomb Memorial Drive
Rochester, NY 14623

Report Documentation Page

Form Approved
OMB No. 0704-0188

1. REPORT DATE	2. REPORT TYPE	3. DATES COVERED
JAN 2013		**00-00-2012 to 00-00-2012**

4. TITLE AND SUBTITLE	5a. CONTRACT NUMBER
Gear Fatigue Diagnostics and Prognostics	5b. GRANT NUMBER
	5c. PROGRAM ELEMENT NUMBER
6. AUTHOR(S)	5d. PROJECT NUMBER
	5e. TASK NUMBER
	5f. WORK UNIT NUMBER
7. PERFORMING ORGANIZATION NAME(S) AND ADDRESS(ES) **Rochester Institute of Technology,111 Lomb Memorial Drive,Rochester,NY,14623**	8. PERFORMING ORGANIZATION REPORT NUMBER
9. SPONSORING/MONITORING AGENCY NAME(S) AND ADDRESS(ES)	10. SPONSOR/MONITOR'S ACRONYM(S)
	11. SPONSOR/MONITOR'S REPORT NUMBER(S)

12. DISTRIBUTION/AVAILABILITY STATEMENT
Approved for public release; distribution unlimited

13. SUPPLEMENTARY NOTES

14. ABSTRACT

15. SUBJECT TERMS

16. SECURITY CLASSIFICATION OF:			17. LIMITATION OF ABSTRACT	18. NUMBER OF PAGES	19a. NAME OF RESPONSIBLE PERSON
a. REPORT	b. ABSTRACT	c. THIS PAGE			
unclassified	**unclassified**	**unclassified**	**Same as Report (SAR)**	**21**	

Gear Fatigue Diagnostics and Prognostics
Progress Report

Introduction

This progress report covers the first period of funding (April 2012-September 2012).

The first objective was to collect meaningful gear fault progression data starting from healthy NASA-designed spur test gears and ending with failed parts. Because tooth breaking gives rise to catastrophic failures of larger systems that employ gearboxes, the focus was placed on this failure mode. Data has been collected with the development of prognostic algorithms in mind. With previously designed, fabricated, and instrumented fixtures (one for single gear tooth fatigue, and one for gear-on-gear dynamometer-based tester) we have been collecting crack initiation and crack propagation data. Acoustic emission (AE) sensors, with the accompanying signal processing and software, furnished by VTD, has been added to both fixtures (one at a time) to collect acoustic emission data in parallel with the existing signals: force, displacement, and crack-propagation data (single-tooth fatigue tester); and torque, angular speed, vibration, temperature, and crack-propagation (gear-on-gear dynamometer-based tester).

The main outcome of the study will be a database with raw data, accompanying computed condition indicators (CIs), and photographs. In addition, the developed tools for processing the data, viewing the data, and modifying the data in the database will also be included, with associated documentation.

The current effort is a continuation of the work that was performed under Award No. W911NF-09-2-0002. The prior work included development of fixtures, the first version of the algorithms, methods, and procedures for crack initiation and crack propagation, and preliminary database design.

Test Description

The test consists of two set of tests on a dynamometer and one set of test on the fatigue tester and some additional activities. Fig. 1 shows the flowchart of the testing process.

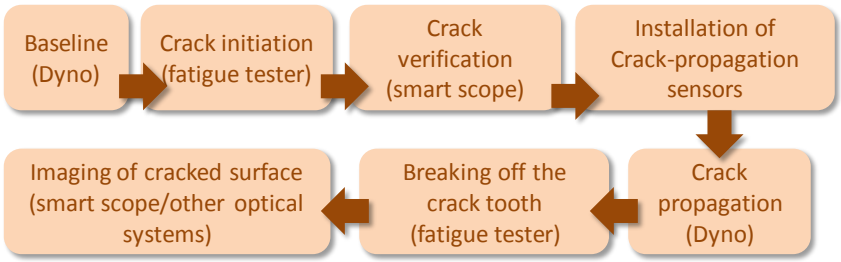

Fig. 1. The flowchart of the testing process.

Two gears are spun together in a gear box according to a torque and angular speed profiles, as shown in Fig. 2. This establishes the baseline for the test. After that the top gear is removed from the gearbox, mounted in the single-tooth, fatigue-tester fixture and the crack is initiated. After the crack is initiated the gear is equipped with two crack-propagation sensors, one at each faces of the cracked tooth. The gear is then re-assembled in the gear box and the gearbox is operated according to the profile shown in Fig. 2, until all the crack is propagated beyond the range of both crack-propagation sensors. After that, tooth is broken off on the fatigue tester using a large load, and the bottom image of the tooth is imaged.

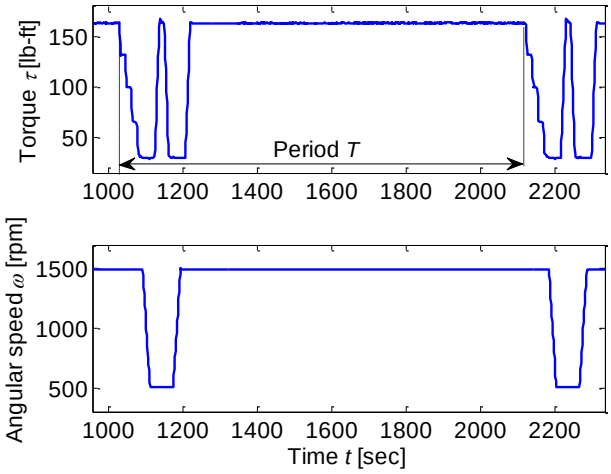

Fig. 2. The segment of the dynamometer operating conditions, viz. torque τ and angular speed ω. The repeating cycle is indicated in the graph with T.

Crack initiation

Fatigue-tester-based, single-tooth fixture is shown in Fig. 3. An anvil applies a normal force approximately at the highest point of single tooth contact (HPSTC). The fixture was designed and built before the current project, under Award No. W911NF-09-2-0002. When used for this project, the fixture employed *soft anvil*, i.e. anvil made of material considerably softer than the gear. Such anvil conforms to the gear during the test, but does not cause any visible indentation of the surface of the involute that could add its own vibration signature.

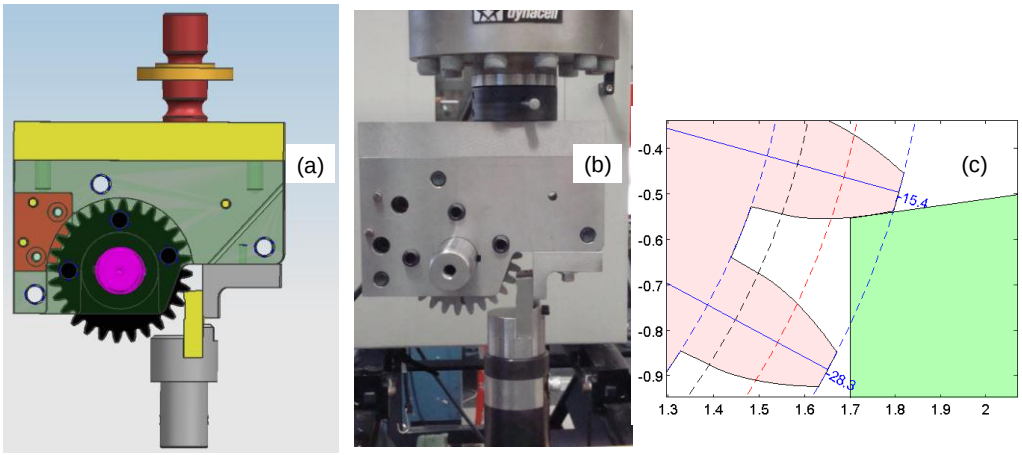

Fig. 3: Fatigue-tester-based, single-tooth fixture. (a) CAD model (b) Photo of the built fixture. (c) The force is applied approximately perpendicularly at HPSTC.

The inference engine used to stop the fatigue cycling fatigue tester operates on observation of force and displacement. A baseline distribution is obtained from using a compliance-based feature described in [1]. The feature is then observed for set of samples that are delayed with respect to the most recent observations, and the baseline normal distribution is estimated. Once the baseline distribution is available, a set of recent samples is assessed whether it belongs to this distribution using a likelihood ratio, as illustrated in Fig. 4. The signals are shown in Fig. 4a: the blue trace shows the feature, while the red trace shows the threshold based on baseline distribution. When the feature crosses the threshold, the test is stopped. Fig. 4b and Fig. 4c show the cracks verified in a non-destructive manner, using magnetic die penetrant and ultraviolet (UV) light.

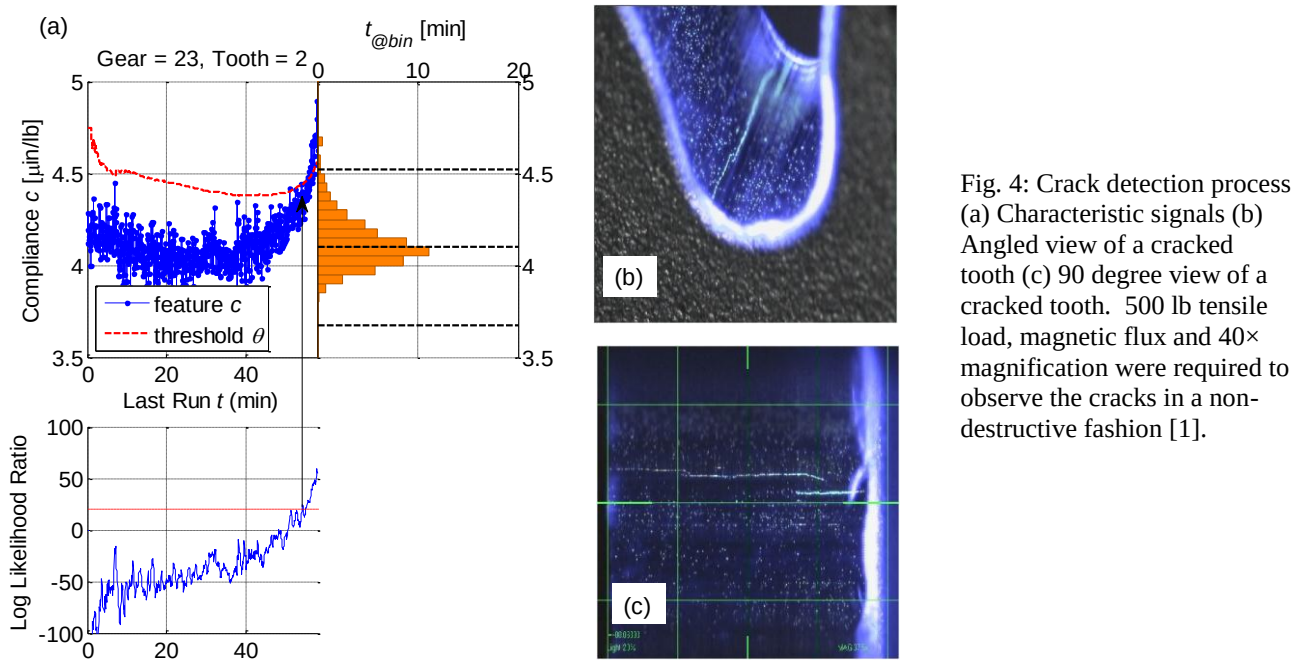

Fig. 4: Crack detection process (a) Characteristic signals (b) Angled view of a cracked tooth (c) 90 degree view of a cracked tooth. 500 lb tensile load, magnetic flux and 40× magnification were required to observe the cracks in a non-destructive fashion [1].

The resolution of the feature has recently been improved. Table 1 shows a subset of the series of test that compared the threshold parameter to the resulting initiated crack. The threshold parameter θ is expressed as the number of standard deviations σ of the baseline distribution. As

before, the blue traces in the plots indicate the features, while the red traces indicate the thresholds. The associated images show the tooth side of the crack. It is important to note that the crack measurement, indicated in the plots, are the normal projections, not the actual crack lengths that are typically slightly longer. As this subset shows, the initiated cracks vary considerably in size and shape. Some cracks are even discontinuous and initiate at different planes.

Dimensions of NASA gear in mm are provided to facilitate the assessment of the relative sizes of the cracks.

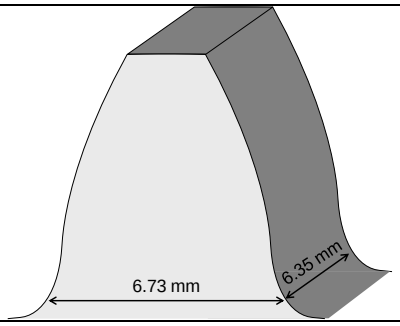

Table 1: Excerpt from detailed comparison of performance of crack-initiation method. GearID

Threshold $\theta = 6.5\times\sigma$		Threshold $\theta = 6.0\times\sigma$	
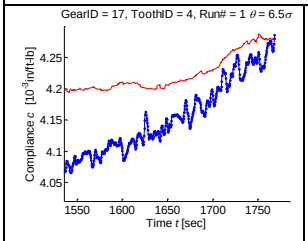	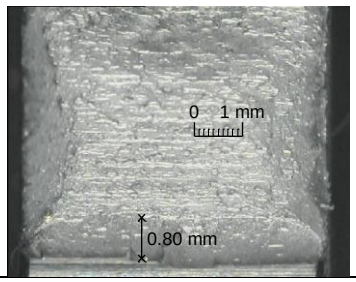	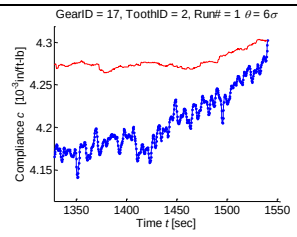	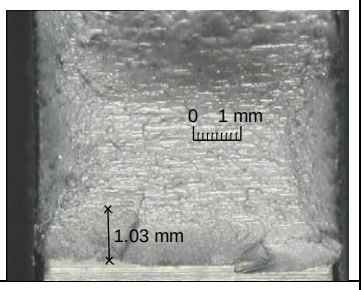
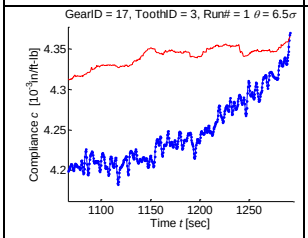	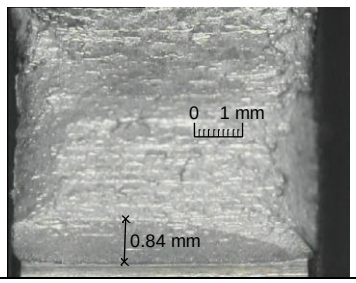	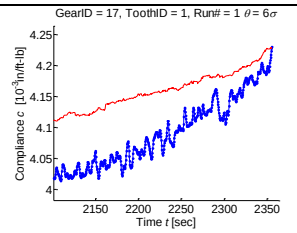	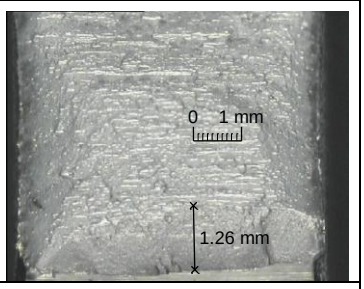
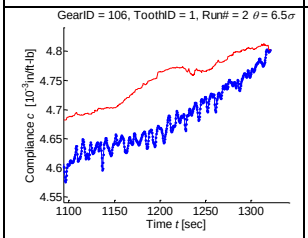	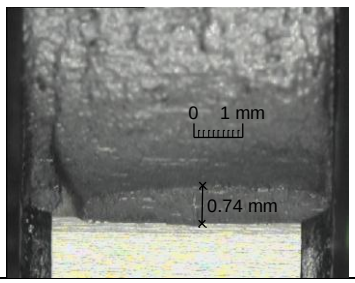	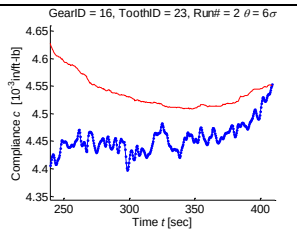	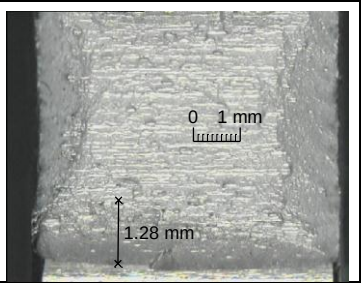

After a cracks is initiated, the cracked tooth is instrumented with two crack propagation sensors, as shown in Fig. 5.

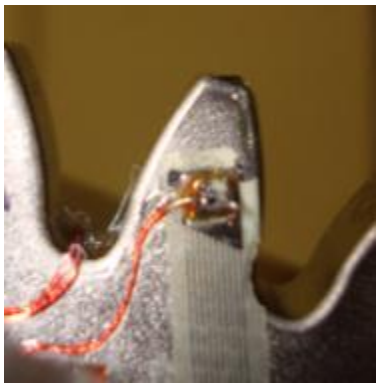

Fig. 5. A gear tooth equipped with crack propagation sensors after crack initiation.

Crack Propagation

Dynamometer fixture is shown in Fig. 6. The fixture is instrumented with four accelerometers. Some of these are placed at locations very sensitive to gear cracks, and some at locations that are expected to have relatively poor sensitivity to gear crack. Sub-optimal placement was motivated by the fact that one must use pragmatic, sub-optimal sensor placement in practical applications due to space and other constraints.

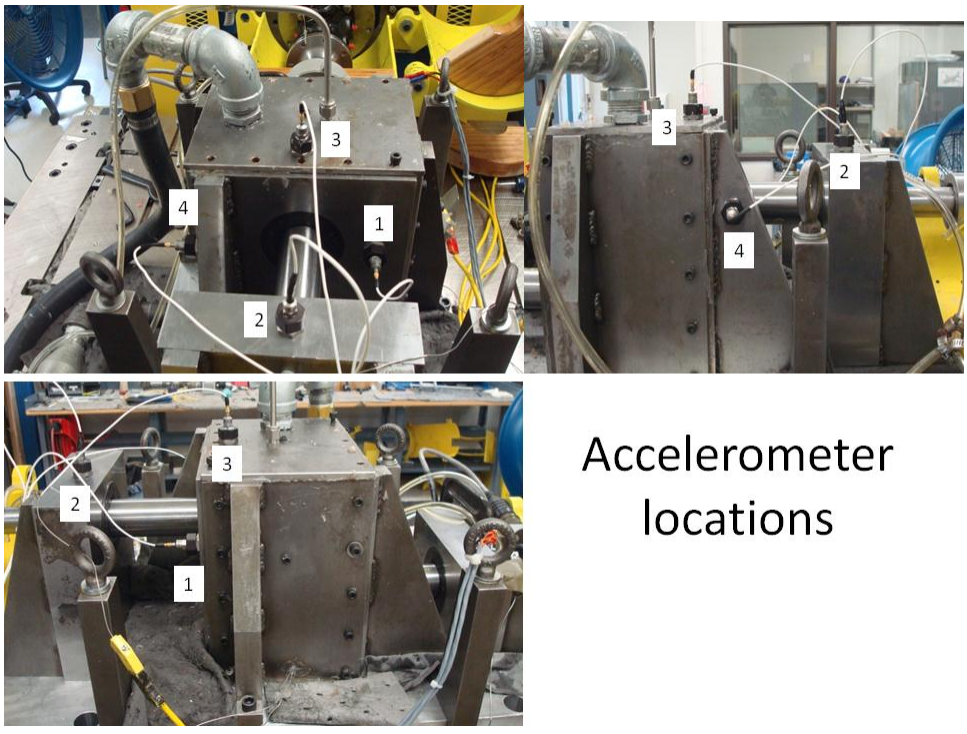

Fig. 6. Dynamometer test stand (gearbox) with the location of the accelerometers.

The instrumentation of the control and the data acquisition system is implemented in LabVIEW. Fig. 7. shows a block diagram of the system. Most of the low-level control is achieved via Mustang software. Accelerometer data is collected from four accelerometers (PCB 352A60), amplified using a PCB amplifier and further filtered and amplified using 8th-order anti-aliasing filters (LTC1564) with 40 kHz cut-off frequency. The signals from crack-propagation sensors (CG1 and CG2) are wired through the slip rings, passed through anti-aliasing filters and

amplified. Their referenced, single-ended, analog inputs were used to track crack growth as individual strands in the gage break. Gages were applied to both faces of the pre-cracked gear tooth. High speed sampling is needed to measure peak load on a single tooth each revolution. Digital encoder pulses read into an analog input to provide a signal for Time Synchronous Averaging (TSA). The timer digital input (counter/timer) was used to measure time between pulses and to compute gear speed in revolutions per minute. The encoder pulses were also accumulated in a digital counter and used to track total gear loading cycles during a test run. A digital output signal is set when limits are exceeded for crack length, maximum accelerometer RMS, or the number of revolutions. The digital output from the LabVIEW monitor application is connected to the Mustang Dynamometer "shutdown" digital input port, and will cause a test shutdown when enabled. The new feature of the instrumentation is the ability to collect the triggers of the AE events. Acoustic emission signals were captured from the trigger of the Digital Wave FM-1 AE detector.

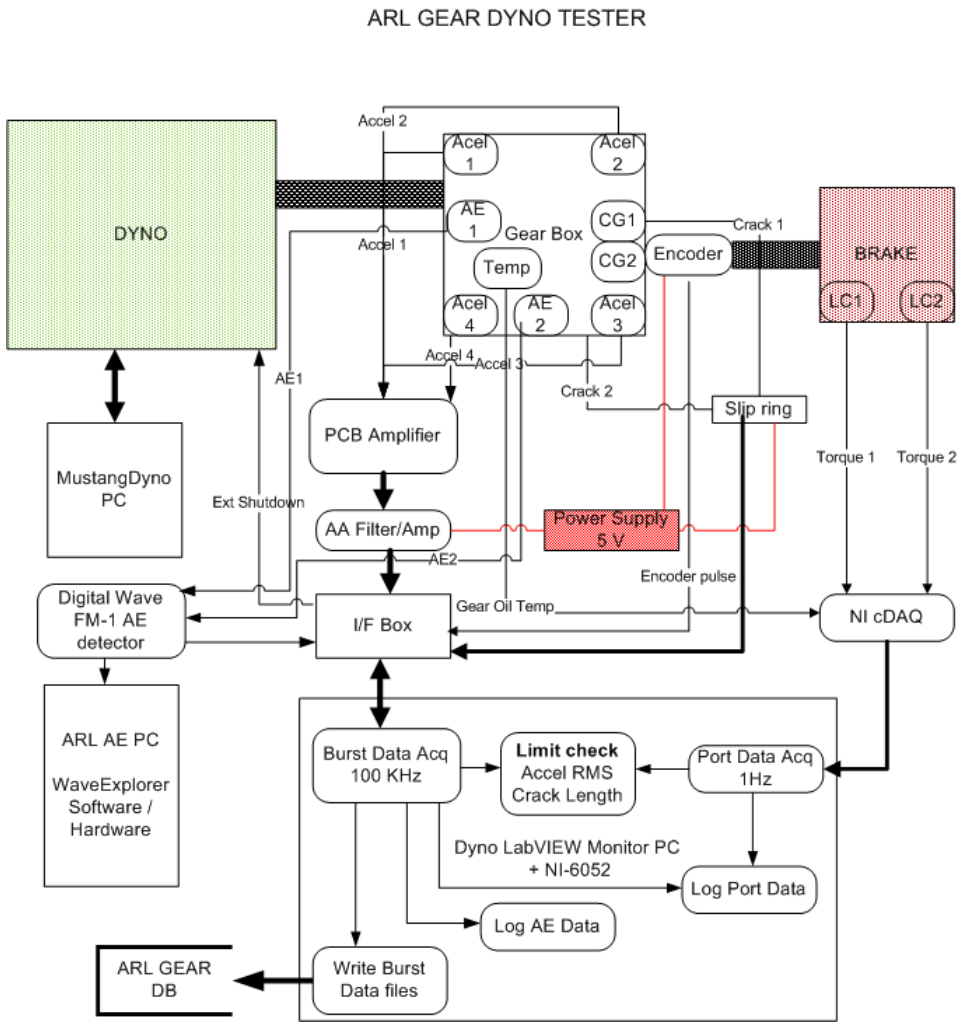

Fig. 7. Block diagram of the instrumentation system associated with the dynamometer fixture.

Acoustic Emission Testing

Acoustic emission (AE) was collected during single-tooth testing, i.e. crack initiation and propagation on the fatigue tester, and during crack propagation on the gearbox testing. The AE sensor placement on the single-tooth fatigue fixture is shown in Fig. 8.

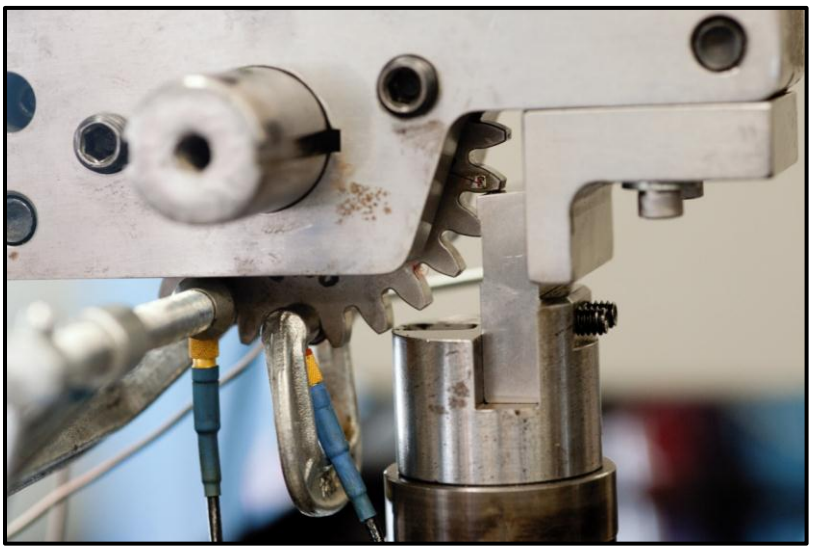

Fig. 8. Close-up of AE instrumentation of the single-tooth fatigue fixture. This image is credited to Dr. Adrian Hood of ARL.

Several crack initiation and propagations were ran on this fixture and the AE signals are performed and the frequency of AE events were related to crack-propagation signals (CP).

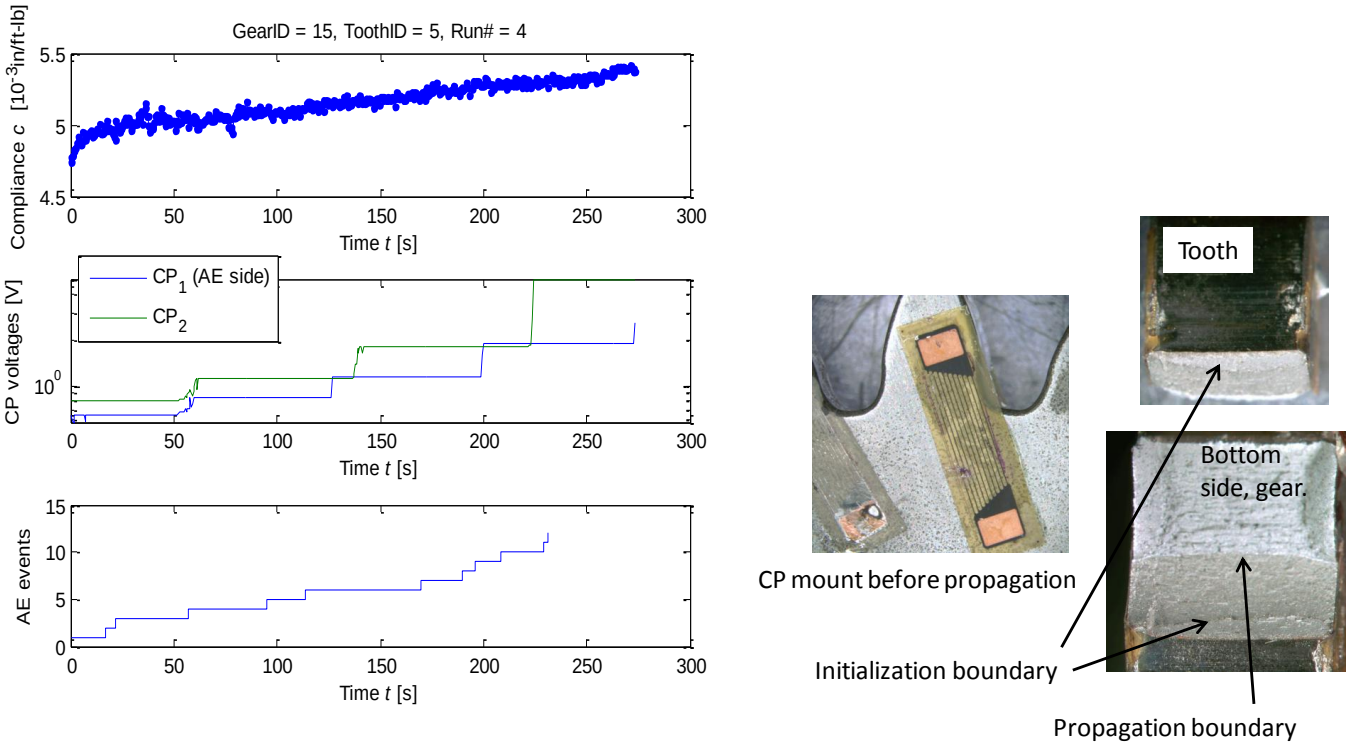

Fig. 9. Crack propagation on the fatigue tester (a) relating AE signals to CP signals and the compliance feature (b) Images of the tooth after crack initiation and crack propagation.

The cracks were propagated at 100-1500 lbs cyclic load at 10 Hz. The DAQ system of the

acoustic emissions sensors continuously sampled data in bursts of 8192 points sampled at 10 MHz. The data was continuously discarded until a threshold was reached. When reached, an EVENT was logged and the current burst, along with 819 points from the previous burst were saved.

Fig. 8a shows the waveforms of the compliance feature, crack propagation signals, and the cumulative graph of acoustic events.

Digital Waveform software saves the data in binary files and GIS/RIT built a MATLAB parser for visualization of AE events in the time and frequency domain and cumulating the events during the test. Fig. 10 shows the front panel of the tool with one event in the time domain.

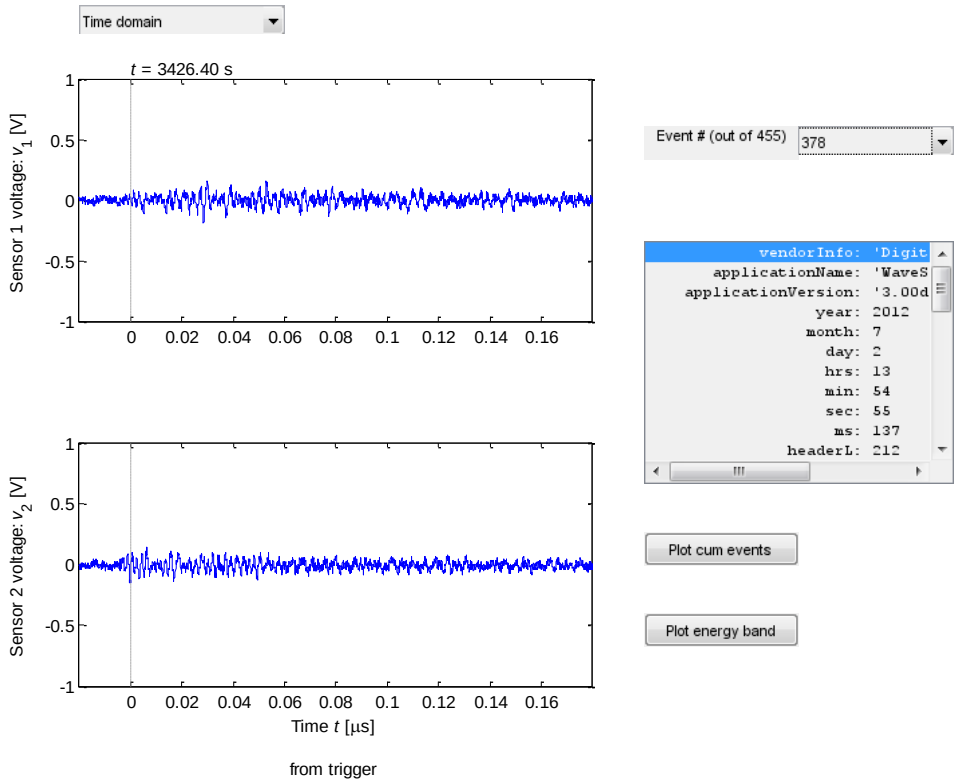

Fig. 10: MATLAB parser for AE data captured by Digital Waveform.

A cumulative plot of all the events for the corresponding test are shown in Fig. 11.

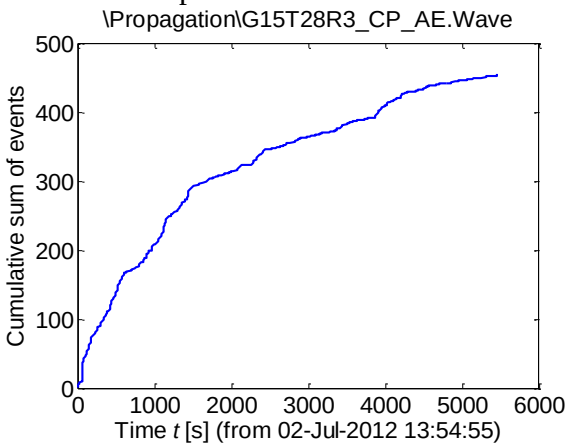

Fig. 11: Cumulative sum of the events for a given test.

AE seem to be very sensitive to the sensor placement. For example, Fig. 12 shows the case where

AE events responds much more once the crack starts to propagate on the face of the tooth on which AE sensors are mounted.

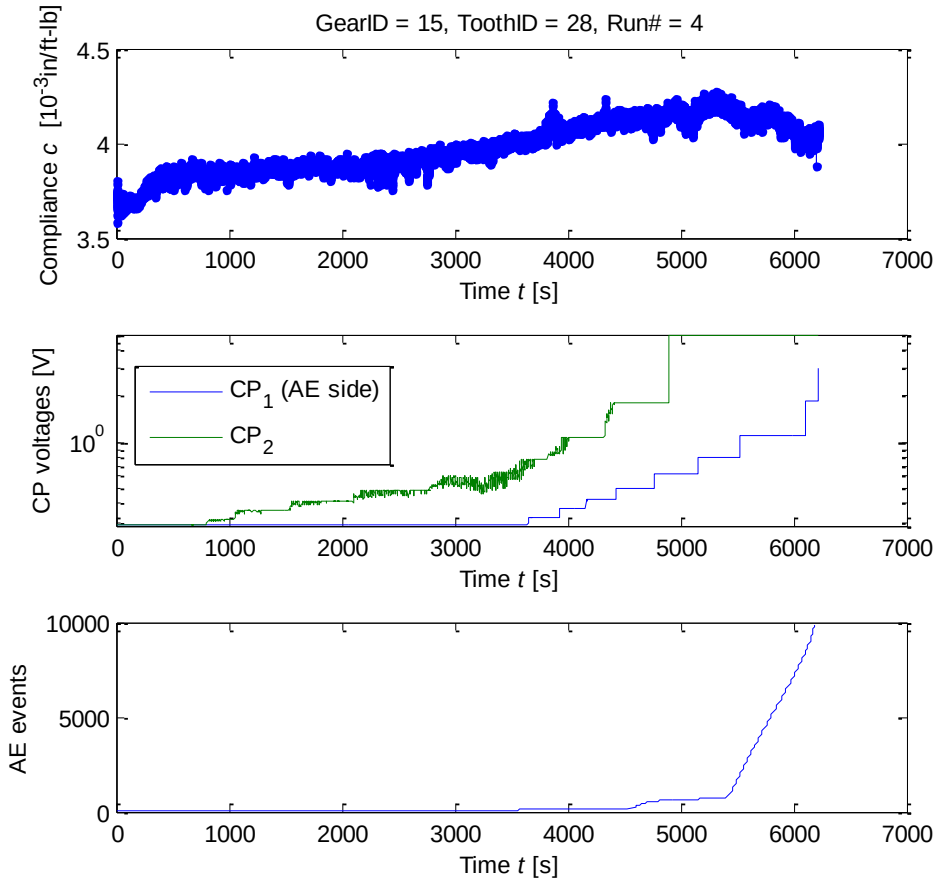

Fig. 12: Propagation with acoustic emission. AE sensors are mounted on the same face of the gear as CP1.

The captures on the dynamometer are currently very noisy. A very large number of events are captured during the baseline tests when the AE equipment settings are set to considerable lowers sensitivity than the settings employed for propagation on the fatigue tester. Thus, acoustic emission detection for the gearbox does not look very promising.

Current Results

Up to this point, we have completed five crack propagations: four on slightly undersized gears and one on the gears that fully meet the specifications. All the database is currently kept in a single database. Fig. 13 shows the tables of the database. This database system also supports the configuration where the binary files containing the high-speed data (accelerometers and encoder) can be read as the linked files using *dyno_test_burst_details* table.

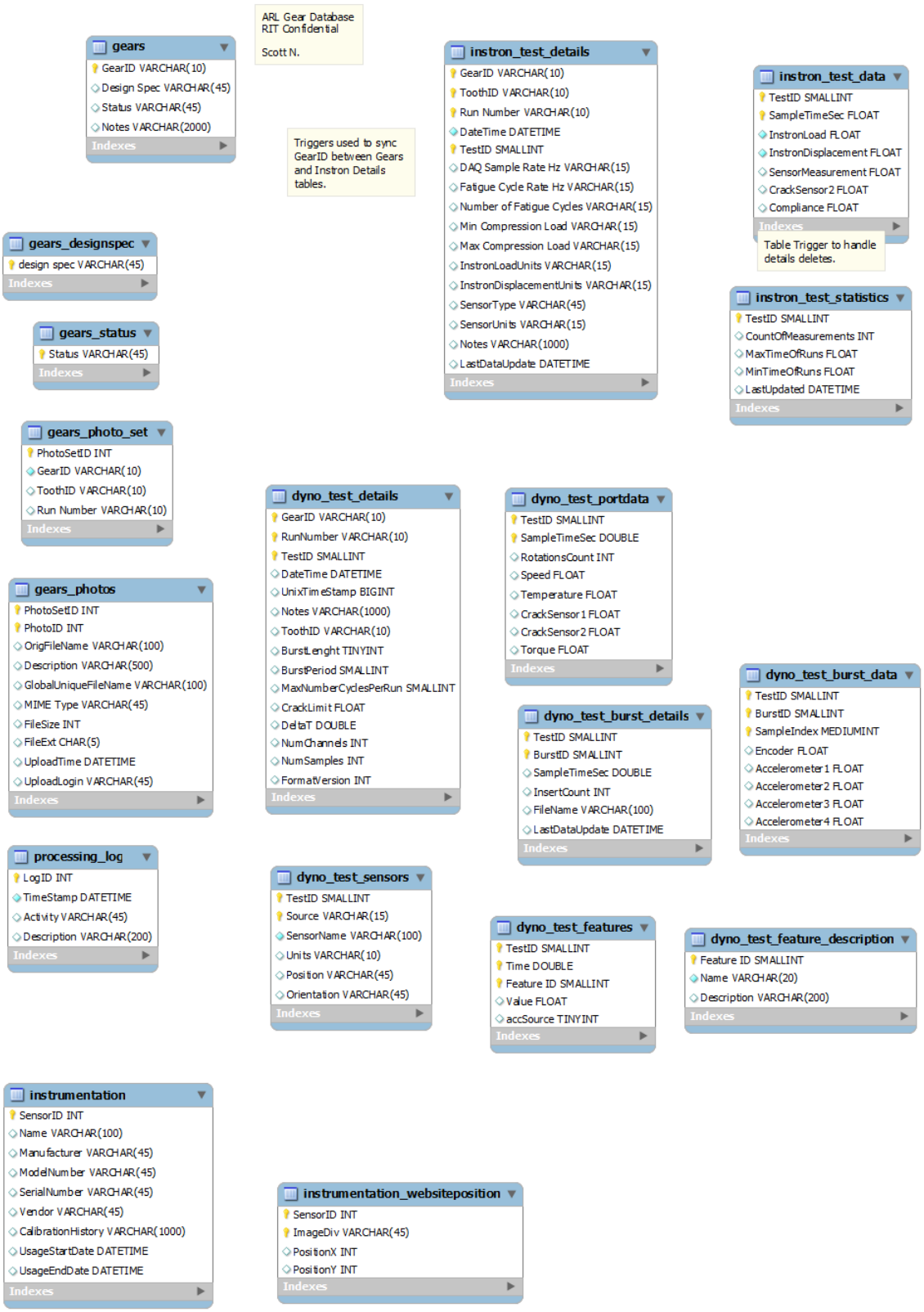

Fig. 13. Database tables used in the test process.

Data viewer in MATLAB is shown in Fig. 14. The user selects the run for a gear. The top subplot shows the angular speed (left, blue axis) and the torque (right, green axis) for the duration of the test. The bottom plot shows the encoder and accelerometer data selected within the interval selected by the red dashed lines in the top plot.

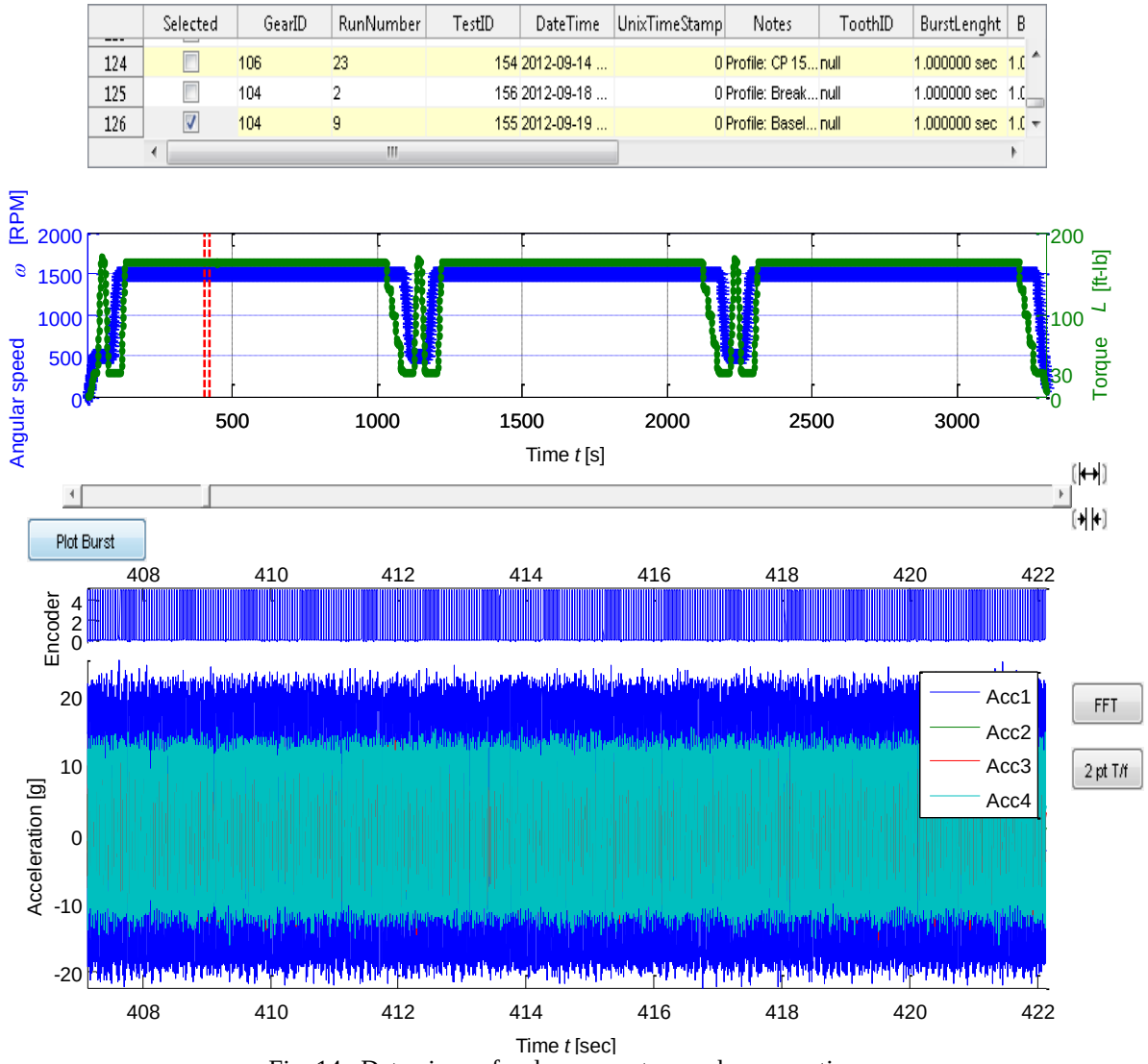

Fig. 14. Data viewer for dynamometer crack propagation.

A zoomed view into the high speed data is shown in Fig. 15.

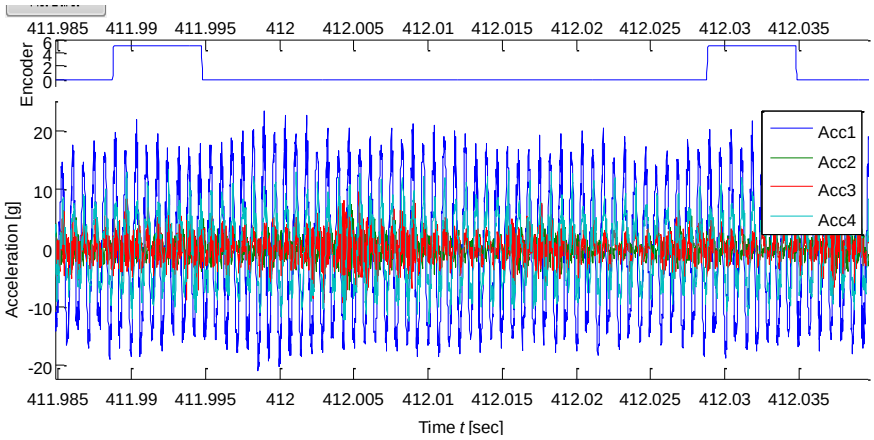

Fig. 15. Zoom into the burst data.

For each crack, the imaging after the full propagation is performed. The top surface o the cracked (the tooth side) of GearID = 106 is shown in Fig. 16. Three different regions are readily distinguishable: crack initiation region, crack propagation, and final, abrupt fracture. The darker region within the surface that corresponds to crack propagation indicates heating of the material, caused by hysteretic losses associated with the crack propagation. We have observed that when this occurs during the plastic deformation, crack propagation can be slowed-down significantly, and even halted entirely. In this particular test, the propagation on the dynamometer took considerable number of cycles.

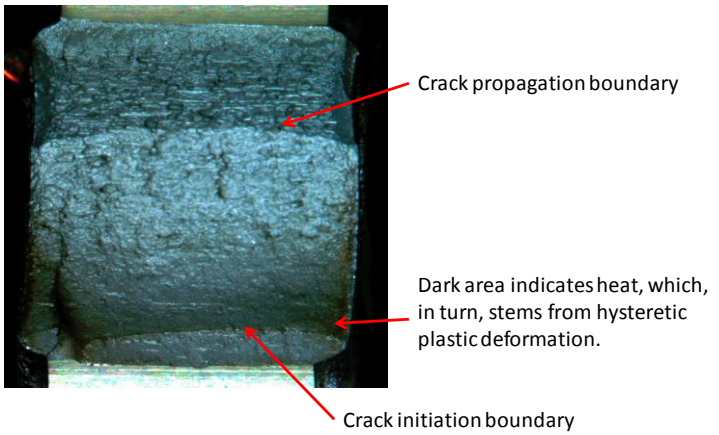

Fig. 16. The bottom surface of a cracked tooth (GearID = 106). Three different regions (crack-initiation, crack-propagation, and final fracture) are readily distinguishable.

Refer to Table 1, the first column and the bottom row for the measurement of projection of crack-initiation.

Fig. 17 shows a set of images associated with crack initiation and crack propagation on a different gear (GearID = 3). In this case the bottom surface of the crack is shown (the gear side instead of the tooth side). Again the three regions (crack-initiation, crack-propagation, and final fracture) can be observed.

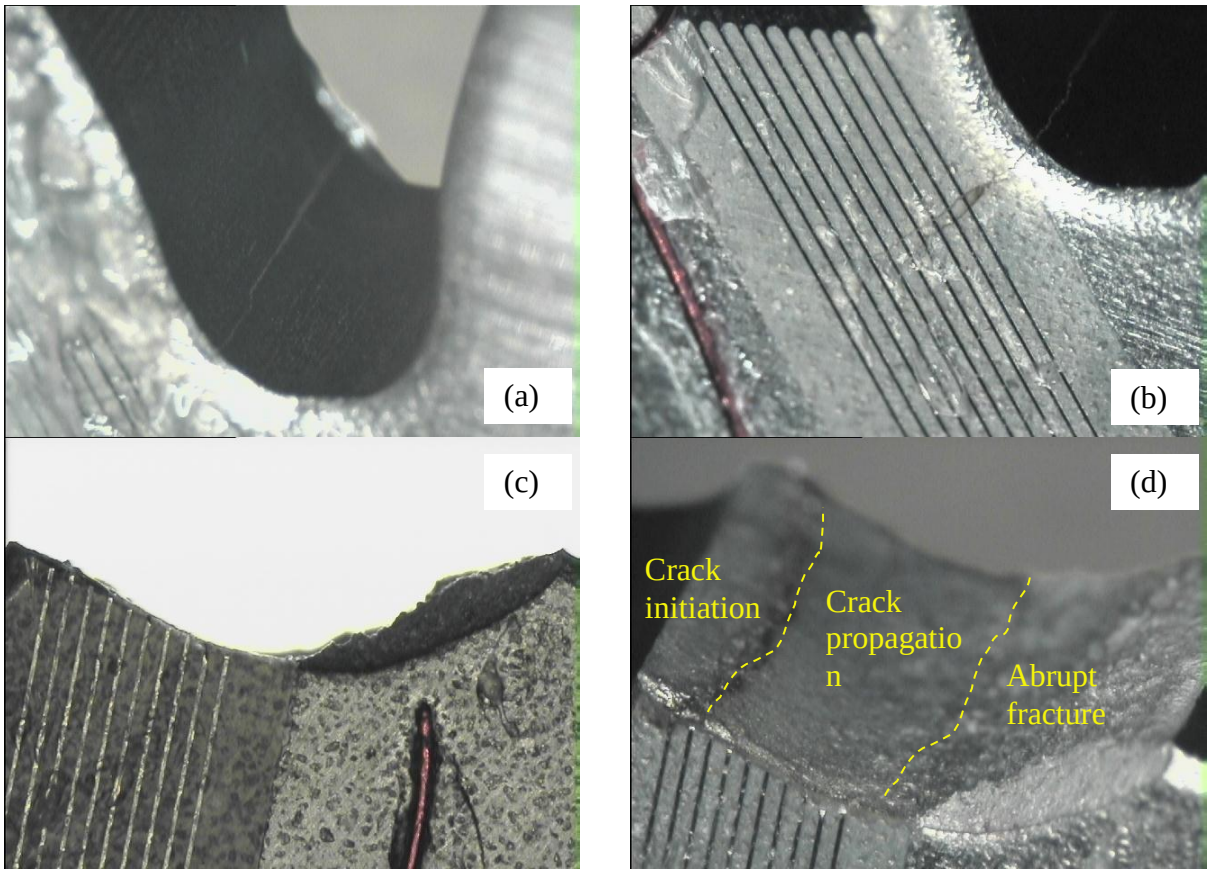

Fig. 17: Images of failed tooth (a) crack initiation (b) crack propagation – the crack propagate through all the crack propagation sensor on both sides (c) broken off tooth (d) image of the crack surface

Analysis of Condition Indicators (CIs)

In this report we use the term *feature* and *condition indicator* (CI) interchangeably. While the data tables are read only, the tables containing condition indicators and their descriptions can be overwritten by the analyst, to enable re-computing of existing features, and introduction of new features. The analyst can introduce new features, assign them a feature ID, compute them and add them to *dyno_test_features* table, described in Table 2.

Field	Type	Null	Key	Default	Extra
Feature ID	smallint(6)	NO	PRI	NULL	
TestID	smallint(6)	NO	PRI	NULL	
Time	double	NO	PRI	NULL	
Value	float	YES		NULL	
accSource	tinyint(3) unsigned	NO	PRI	NULL	

Table 2: *dyno_test_features* is a read/write table where features can be re-computed and added.

The features are described in *dyno_test_feature_description* table. Currently we are computing thirty five features. These features are listed in Table 3. In many cases, original papers that describe the features are provided, e.g. [2-8] For the purpose of the present report, only three features are considered: *FM0, NA4*, and *NP4*.

Table 3: List of condition indicators (CI) and their descriptions, as currently described in *dyno_test_feature_description table.*

Feature ID	Name	Description
1	Raw_RMS	Root Mean Square of Signal
2	Raw_Delta_RMS	Change in the Root Mean Square of the signal
3	Raw_Kurtosis	4th Statistical Moment of the signal normalized by the square of the variance of the signal
4	Raw_Crest_Factor	Swansson, N.S. Application of Vibration Signal Analysis Techniques to Signal Monitoring. Conference on Friction and Wear in Engineering 1980. Institution of Engineers, Australia, Barton, Australia, 1980, pp 262-267.
5	TSA_RMS	Root Mean Square of TSA
6	TSA_Delta_RMS	Change in the Root Mean Square of TSA
7	TSA_Kurtosis	4th Statistical Moment of the TSA normalized by the square of the variance of the TSA
8	TSA_Crest_Factor	Swansson, N.S. Application of Vibration Signal Analysis Techniques to Signal Monitoring. Conference on Friction and Wear in Engineering 1980. Institution of Engineers, Australia, Barton, Australia, 1980, pp 262-267.
9	TSA_Energy_Operator	
10	FMO	Stewart, R.M. Some Useful Data Analysis Techniques for Gearbox Diagnostics. Machine Health Monitoring Group, Institute of Sound and Vibration Research, University of Southampton, Report MHM/R/10/77, July 1977.
11	FM4	Stewart, R.M. Some Useful Data Analysis Techniques for Gearbox Diagnostics. Machine Health Monitoring Group, Institute of Sound and Vibration Research, University of Southampton, Report MHM/R/10/77, July 1977.
12	M6As	Martin, H.R. Statistical Moment Analysis As a Means of Surface Damage Detection. Proceedings of the 7th International Modal Analysis Conference, Society for Experimental Mechanics, Schenectady, NY, 1989, pp. 1016-1021.
13	M8A	Martin, H.R. Statistical Moment Analysis As a Means of Surface Damage Detection. Proceedings of the 7th International Modal Analysis Conference, Society for Experimental Mechanics, Schenectady, NY, 1989, pp. 1016-1021.
14	M8As	
15	NA4	Zakrajsek, J.J., Townsend, D.P., Decker, H.J. An Analysis of Gear Fault Detection Methods as Applied to Pitting Fatigue Failure Data. NASA Lewis Research Center/U.S. Army Aviation Systems Command. 47th Mechanical Failure Prevention Group, NASA TM 105950, AVSCOM TR 92-C-035, April 1993.
16	NA4s	Decker, H.J., Handschuh, R.F., Zakrajsek, J.J. An Enhancement to the NA4 Gear Vibration Diagnostic Parameter. U.S. Army Research Laboratory/NASA Glenn Research Center. 18th Annual Meeting of the Vibration Institute, NASA TM 106553, ARL-TR-389, June 1994.
17	NB4	Zakrajsek, J.J., Handschuh, R.F., Decker, H.J. Application of Fault Detection Techniques to Spiral Bevel Gear Fatigue Data. NASA Lewis Research Center/U.S. Army Research Laboratory 48th Mechanical Failures Prevention Group, Wakefield, Mass. April 1994. NASA TM 106467, ARL-TR-345
18	NB4s	Application of difference between NA4 and NA4* to NB4. No paper published.
19	Energy_ratio	Swansson, N.S. Application of Vibration Signal Analysis Techniques to Signal Monitoring. Conference on Friction and Wear in Engineering 1980. Institution of Engineers, Australia, Barton, Australia, 1980, pp 262-267.
20	Filter_RMS_Env	
21	Filter_Kurtosis_Env	
22	Signal_STD_Env	
23	Peak_Frequency_env	
24	Peak_Amplitude_Env	
25	Peak_Amplitude_Demod	
26	Peak_Ampitude_Demod	
27	NP4	Polyshchuk, V.V., Choy, F.K., Braun, M.J. Gear Fault Detection with Time-Frequency based Parameter NP4. Proceedings from the 8th International Symposium on Transport Phenomena and Dynamics of Rotating Machinery (ISROMAC-8), Honolulu, Hawaii, March 26-30, 2000.

Table 3 (continued): List of condition indicators (CI) and their descriptions, as currently described in *dyno_test_feature_description table.*

28	LP2 Kurtosis	Kurtosis of the Linear Predictive Residual using a second-order model
30	LP3 Kurtosis	,Kurtosis of the Linear Predictive Residual using a third-order model
32	LP4 Kurtosis	,Kurtosis of the Linear Predictive Residual using a fourth-order model
33	LP4 L1 Sum	,L1 distance of the Linear Predictive Residual using a fourth-order model
31	LP3 L1 Sum	,L1 distance of the Linear Predictive Residual using a third-order model
29	LP2 L1 Sum	,L1 distance of the Linear Predictive Residual using a second-order model
34	CP Sensor 1	Post-processed crack propagation sensor data, indicating crack length.
35	CP Sensor 2	Post-processed crack propagation sensor data, indicating crack length.

We compare the performance of condition indicators with respect to:

1. Their ability to detect a crack
2. Their ability to assess the damage
3. Their sensitivity to sensor placement.

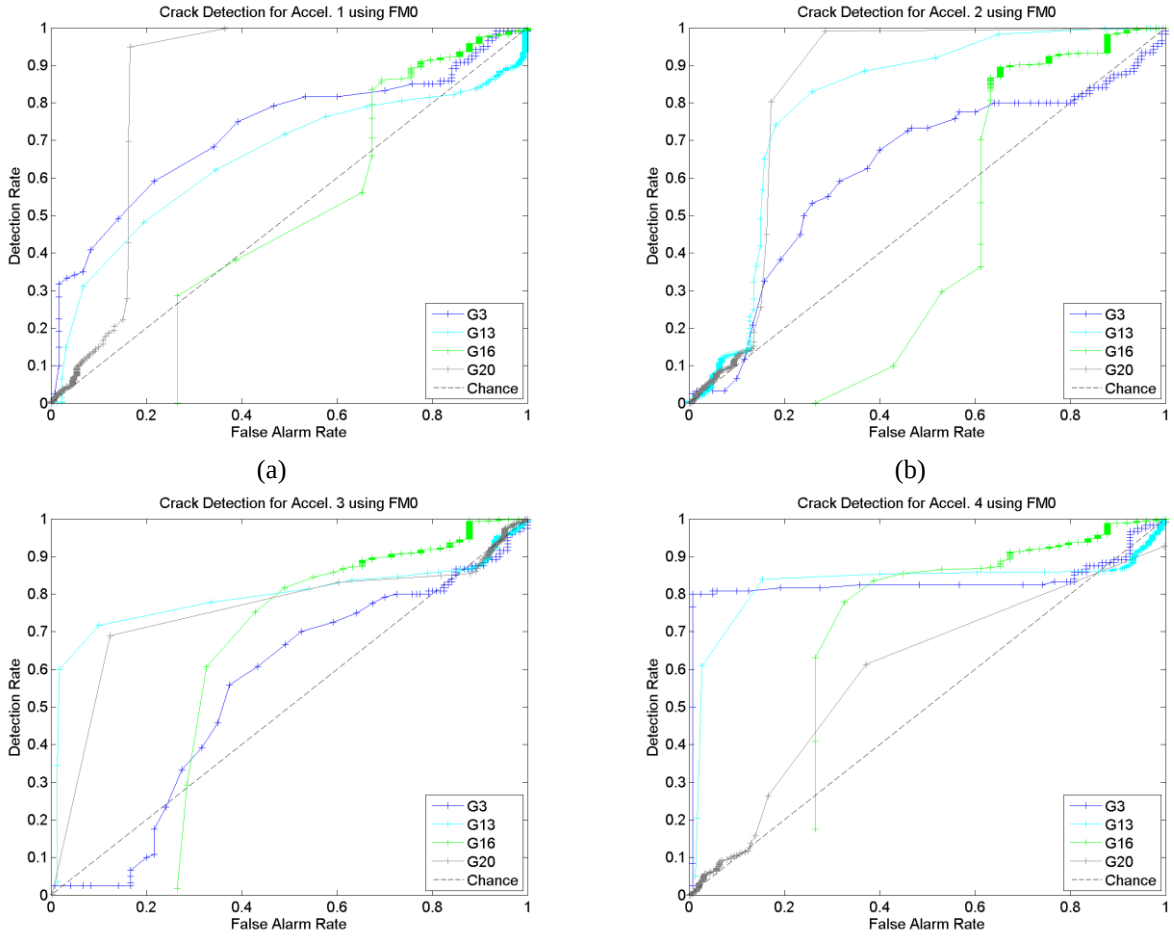

Fig. 18: *FM0* detection using ROC for four accelerometers. (a) Accelerometer 1 (b) Accelerometer 2 (c) Accelerometer 3(d) Accelerometer (4)

Early detection problem. Receiver Operating Characteristic (ROC) is used for comparison of features with respect to their ability to detect the damage. In these plots, the *x*-axis represents the false alarm rate and the *y*-axis represents the detection rate. A larger the area under the curve (AUC) corresponds to a better the performance of the detector. The worst performance is given by the diagonal $x = y$ which represents pure chance, and has AUC = 0.5. More details on ROC can be found in e.g. [9]. To generate the curves, the ground truth was chosen during the baseline interval (no fault) and during the propagation, before the first strand of either crack propagation sensor is broken (fault). Thus, more specifically, we compared the features with respect to their ability for their ability to detect features early.

Fig. 18, Fig. 19, and Fig. 20 show the performance of *FM0*, *NA4*, and *NP4*, respectively. Each gear is represented by a separate trace[1]. Each subplot corresponds to one of the four accelerometers.

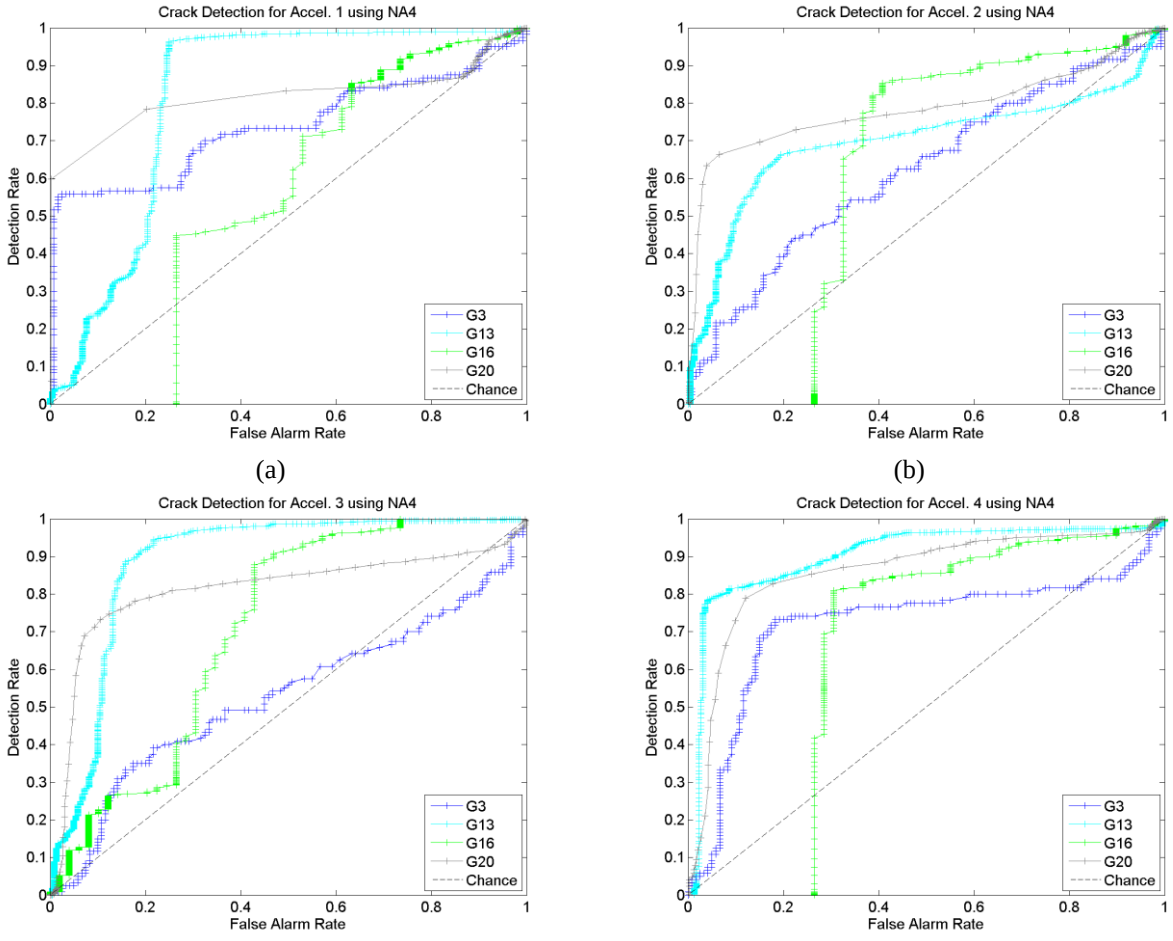

Fig. 19: *NA4* detection using ROC for four accelerometers. (a) Accelerometer 1 (b) Accelerometer 2 (c) Accelerometer 3(d) Accelerometer (4)

Comparing the performance of the accelerometer in Fig. 18-Fig. 20, Accelerometer 4 is consistently the best performer (refer to Fig. 6 for the sensor placement), Accelerometer 3 is

[1] … Of completed crack propagations on the dynamometer fixture, only the propagation of GearID = 106 is not included, because the processing was not able to

consistently the worst, while Accelerometer 2 and Accelerometer 3 are tied in the middle. Of the three features compared here, *NP4* shows the best performance.

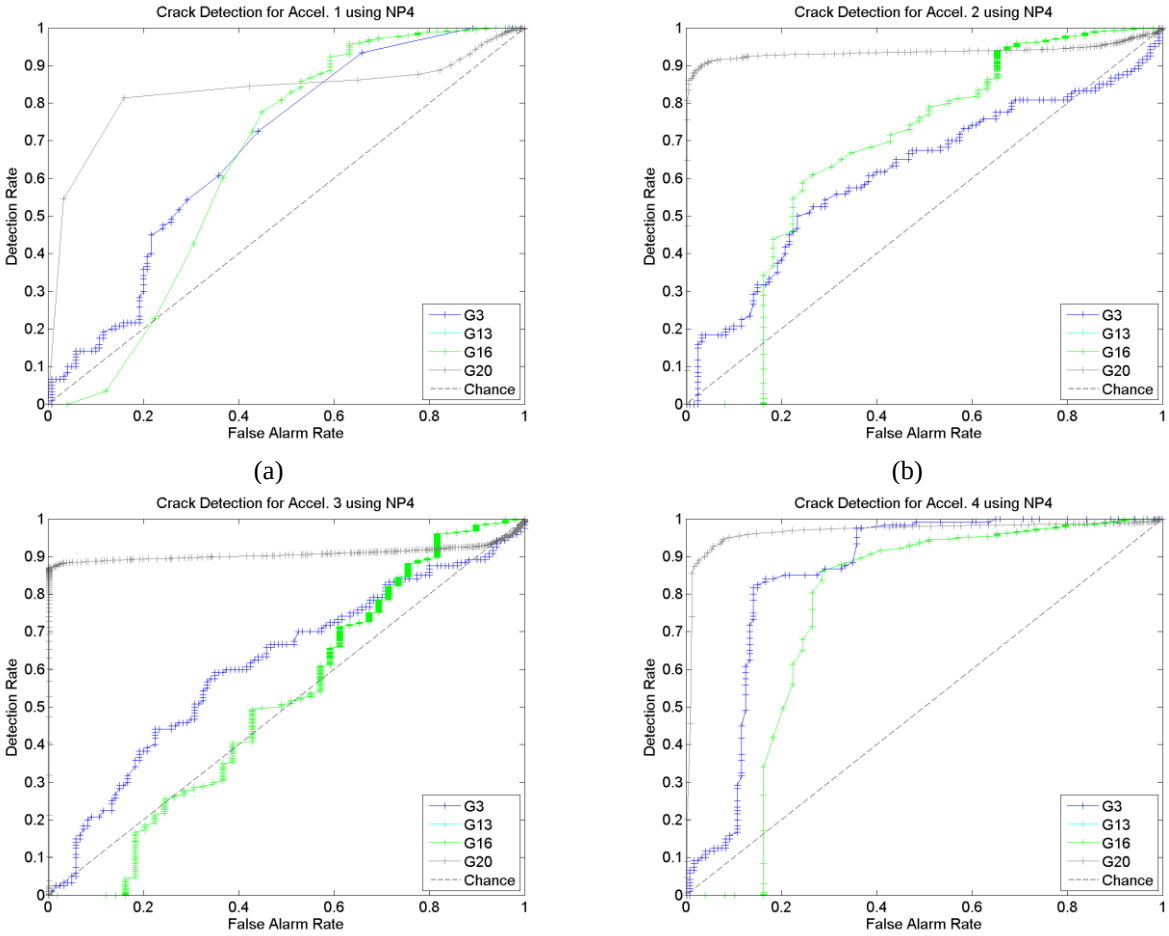

Fig. 20: *NP4* detection using ROC for four accelerometers. (a) Accelerometer 1 (b) Accelerometer 2 (c) Accelerometer 3(d) Accelerometer (4)

Fixture Problems and Delays

During this performance period we have experienced two unexpected equipment-related problems: equipment failure on the dynamometer tester and required modification on the fatigue tester.

Dynamometer Fixture Failure

During a test run on the dynamometer the nylon key between the drive motor coupler and fixture's input shaft sheared. This key is used as the weak link within the system to prevent unnecessary stress in the gearbox due to jamming of a broken tooth and/or shock loads. Additionally, the setscrew constraining the key may have been inserted into the beyond the surface of the shaft. Once the key sheared the setscrew marred the shaft's surface thus preventing easy removal of the mating coupler. Modifications have been made to prevent re-occurrence: a new coupler was designed to allow rotation around the shaft in the event of a

similar break, use of nylon tipped setscrews, and increased key length to decrease bearing stresses.

Modification of the Fatigue Tester

The fatigue fixture was designed according to the specifications and performed well for the slightly-out-of spec (undercut) gears. The gears that fully meet the specification did not easily fit in the fatigue fixture and we had to open the spacing between the reaction teeth, as indicated in the drawing of Fig. 21.

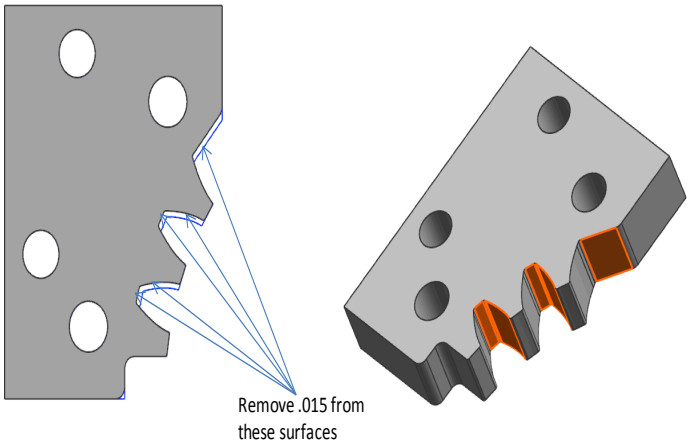

Fig. 21: The fixture modification.

Summary and Future Work

The goal is to proceed with crack initiation and crack propagation with additional gear samples. Due to unexpected failure of the gearbox and unexpected modifications required for the fatigue fixture, we produced fewer crack propagations than expected for this performance period. In addition, due to the delays caused by the aforementioned problems, our spending rate was reduced during this performance period, at about 50 % of what was originally projected for this performance period.

References

[1] N. G. Nenadic, J. A. Wodenscheck, M. G. Thurston, and D. G. Lewicki, "Seeding Cracks Using a Fatigue Tester for Accelerated Gear Tooth Breaking
Rotating Machinery, Structural Health Monitoring, Shock and Vibration, Volume 5." vol. 8, T. Proulx, Ed., ed: Springer New York, 2011, pp. 349-357.

[2] J. J. Zakrajsek, D. P. Townsend, and H. J. Decker, "An Analysis of Gear Fault Detection

Methods as Applied to Pitting Fatigue Failure Data," Cleveland Oh, Technical Memorandum 105950, 1993.
[3] R. M. Stewart, "Some Useful Data Analysis Techniques for Gearbox Diagnostics," Southampton, UK MHM/R/10/77, 1977.
[4] H. R. Martin, "Statistical Moment Analysis As a Mans of Surface Damage Detection," in *Proceedings of the 7th International Modal Analysis Conference*, Schenectady, NY, 1989, pp. 1016-1021.
[5] P. D. Samuel, "A Review of Vibration-Based Techniques for Helicopter Transmission Diagnostics," *Journal of Sound and Vibration*, vol. 282, pp. 475-408, 2005.
[6] F. K. Choy, V. Polyshchuk, J. J. Zakrajsek, R. F. Handschuh, and D. P. Townsend, "Analysis of the effects of surface pitting and wear on the vibration of a gear transmission system," *Tribology International*, vol. 29, pp. 77-83, 1996.
[7] H. J. Decker, R. F. Handchuh, and J. J. Zakrajsek, "An Enhancement to the NA4 Gear Vibration Diagnostic Parameter," Clevelend Oh, Technical Memornadum/Technical Report NASA TM 106553/ARL-TR-389, 1994.
[8] N. S. Swanson, "Application of Vibration Signal Analysis Techniques to Signal Monitoring," in *Conference on Friction and Wear Engineering*, Barton, Australia, 1980, pp. 262-267.
[9] R. O. Duda, P. E. Hart, and D. G. Stork, *Pattern classification*, 2nd ed. New York: Wiley, 2001.